




Rhombohedral $\text{Li}_{2.4}\text{Na}_{0.6}\text{V}_2(\text{PO}_4)_3@C$ nanoplates as high-rate and long-life cathode materials for lithium-ion batteries

Meng Li¹, Zonglin Zuo¹, Jianqiu Deng^{1,2,*} , Qingrong Yao^{1,2}, Zhongmin Wang^{1,2}, Huaiying Zhou^{1,2}, and Guanghui Rao^{1,2}

¹School of Materials Science and Engineering, Guilin University of Electronic Technology, Guangxi 541004, Guilin, China

²Guangxi Key Laboratory of Information Materials, Guilin University of Electronic Technology, Guangxi 541004, Guilin, China

Received: 18 December 2017

Accepted: 4 April 2018

Published online:
18 April 2018

© Springer Science+Business
Media, LLC, part of Springer
Nature 2018

ABSTRACT

Rhombohedral $\text{Li}_{2.4}\text{Na}_{0.6}\text{V}_2(\text{PO}_4)_3@C$ nanoplates are synthesized by a simple sol–gel method. The almost single rhombohedral phase nature of $\text{Li}_{2.4}\text{Na}_{0.6}\text{V}_2(\text{PO}_4)_3@C$ along with nanoplate structure leads to high specific capacity and rate capability, and a remarkable cycling performance. As cathode materials for lithium-ion batteries, rhombohedral $\text{Li}_{2.4}\text{Na}_{0.6}\text{V}_2(\text{PO}_4)_3@C$ nanoplates deliver a high initial discharge capacity of 121.6 mAh g^{-1} and an excellent capacity retention of 95.6% after 200 cycles at a rate of 1 C in a potential range of 3.0–4.3 V. Even at a high rate of 10 C, an initial discharge capacity of 115.3 mAh g^{-1} and a capacity retention of 76.7% after 500 cycles are observed. The outstanding electrochemical performance is attributed to the synergetic effect of stable rhombohedral phase, nanoplate structure and uniform carbon coating layer.

Introduction

Rechargeable lithium-ion batteries (LIBs) have been used in hybrid electric vehicles (HEVs), electric vehicles (EVs) and portable electronic equipment owing to their high voltage, high energy density and excellent cycling life [1–3]. Recently, lithium transition metal phosphates such as LiFePO_4 [4, 5], LiMnPO_4 [6, 7], LiCoPO_4 [8] and $\text{Li}_3\text{V}_2(\text{PO}_4)_3$ [9–12] have attracted a great interest as potential cathode materials for lithium-ion batteries. The NASICON-structured $\text{Li}_3\text{V}_2(\text{PO}_4)_3$ has been synthesized in two

different crystallographic structures: the monoclinic $\text{Li}_3\text{V}_2(\text{PO}_4)_3$ (M-LVP) and rhombohedral $\text{Li}_3\text{V}_2(\text{PO}_4)_3$ (R-LVP) [13, 14]. For the M-LVP, a three-dimensional structure is composed of slightly distorted PO_4 tetrahedral and VO_6 octahedral by sharing the oxygen vertexes [13]. The M-LVP has several advantages, including high operating voltage, ionic mobility and theoretical specific capacity (197 mAh g^{-1}). As a cathode material, the M-LVP displays three voltage plateaus in charge–discharge curves corresponding to extraction/insertion of two lithium ions in a potential range of 3.0–4.3 V [15]. In contrast to the

Address correspondence to E-mail: jqdeng@guet.edu.cn

M-LVP, the R-LVP shows only a single voltage platform at 3.75 V, corresponding to the V^{3+}/V^{4+} redox couple [14, 16]. The theoretical capacity of the R-LVP is 133 mAh g^{-1} , corresponding to extraction/insertion of two lithium ions. The R-LVP with a single operation potential and considerable capacity is very attractive because it can supply a stable output power for electronic devices and electric vehicles to run well. Compared with the M-LVP, however, it is very difficult to directly synthesize the R-LVP due to its poor stability. [17–19]. Up to now, several feasible methods have been proposed to obtain rhombohedral compounds [16, 18, 20]. For example, Nazar's and Goodenough's groups have synthesized the R-LVP via chemical ion-exchange method [16, 18]. The partial substitution of metal Na^+ ions for Li^+ ions in pristine LVP can obtain $\text{R-Li}_{3-x}\text{Na}_x\text{V}_2(\text{PO}_4)_3$ (R-LNVP) by stabilizing the rhombohedral structure [20]. Nevertheless, the electrochemical performance of the R-LVP or R-LNVP as cathode materials is usually poor, which restricts their practical application in lithium-ion batteries.

Recently, a few strategies have been applied to improve the electrochemical performance of R-LVP or R-LNVP, such as carbon coating [14] and nano-sized particles [19, 21]. Yao's group has synthesized carbon-coated R-LVP by ion-exchange reaction as a cathode material for lithium-ion batteries, which shows the reversible capacities of 97.7 and 76 mAh g^{-1} at 2 C and 5 C, respectively, and a capacity retention of 77% after 300 cycles at a rate of 1 C [14]. Zhang et al. [19] have prepared porous nanosheet-structured rhombohedral $\text{Li}_2\text{NaV}_2(\text{PO}_4)_3/\text{C}$ using a facile sol–gel method. This $\text{Li}_2\text{NaV}_2(\text{PO}_4)_3/\text{C}$ cathode displays a remarkable high rate capability (80 mAh g^{-1} at 5 C and 68 mAh g^{-1} at 10 C) and long-term cyclability. (About 93% of the initial capacity is retained over 500 cycles at 2 C.) However, the electrochemical performance, especially high-rate performance, cannot meet the requirement of their practical applications in lithium-ion batteries and needs to be further enhanced.

In this paper, rhombohedral $\text{Li}_{2.4}\text{Na}_{0.6}\text{V}_2(\text{PO}_4)_3@\text{C}$ (R-LNVP) nanoplates were successfully synthesized through a simple sol–gel method. The synthesized rhombohedral $\text{Li}_{2.4}\text{Na}_{0.6}\text{V}_2(\text{PO}_4)_3@\text{C}$ nanoplates as cathode materials have a remarkable electrochemical performance with excellent rate capability and long cycle life, delivering an initial discharge capacity of 121.6 mAh g^{-1} and a capacity retention of 95.6% after 200 cycles at 1 C rate in a potential range of 3.0–4.3 V.

Even at a high rate of 10 C, the initial discharge capacity is 115.3 mAh g^{-1} and keeps 76.7% after 500 cycles.

Experimental

Preparation of the materials

Rhombohedral $\text{Li}_{2.4}\text{Na}_{0.6}\text{V}_2(\text{PO}_4)_3@\text{C}$ (R-LNVP) nanoplates were synthesized via a simple sol–gel method. In a typical procedure, stoichiometric amount of NH_4VO_3 , $\text{C}_2\text{H}_2\text{O}_4\cdot\text{H}_2\text{O}$, $\text{LiOH}\cdot\text{H}_2\text{O}$, $\text{NH}_4\text{H}_2\text{PO}_4$, Na_2CO_3 and glucose was dissolved in 50 mL of deionized water under vigorous stirring at 70 °C, and the mixed solution was stirred continually till the green precursor gel was obtained. The obtained precursor gel was dried in a vacuum oven at 120 °C for 12 h to achieve a dry gel. Afterward, the dried precursor was pre-annealed at 350 °C for 4 h and then calcined at 750 °C for 10 h in an atmosphere of Ar gas containing 10% H_2 to yield black R-LNVP nanoplates. Hybrid-phase $\text{Li}_{2.4}\text{Na}_{0.6}\text{V}_2(\text{PO}_4)_3@\text{C}$ (H-LNVP) nano/microspheres were prepared by a solvothermal method using NH_4VO_3 , oxalic acid and polyvinylpyrrolidone (PVP) as starting materials. First, PVP was dissolved in 80 mL of ethylene glycol, and 0.01 mol NH_4VO_3 and 0.015 mol $\text{C}_2\text{H}_2\text{O}_4\cdot\text{H}_2\text{O}$ were added to the mixed solution under vigorous stirring at 70 °C. Stoichiometric $\text{LiOH}\cdot\text{H}_2\text{O}$, $\text{NH}_4\text{H}_2\text{PO}_4$ and Na_2CO_3 dissolved completely into the mixed solution. The amount of PVP was based on 10 wt% residual carbon in $\text{Li}_{2.4}\text{Na}_{0.6}\text{V}_2(\text{PO}_4)_3@\text{C}$. Then, the mixed solution was transformed into a 100-mL Teflon-lined stainless steel autoclave and heated at 180 °C for 2 h. After the solution cooled to room temperature, the solution was dried at 80 °C until the ethylene glycol was completely vaporized and dried at 120 °C for 12 h in a vacuum oven to achieve the precursor powders. Here, PVP not only served as a template, but also acted as a carbon source to enhance the electronic conductivity of $\text{Li}_{2.4}\text{Na}_{0.6}\text{V}_2(\text{PO}_4)_3$. The sintering process was same as the synthesis of R-LNVP nanoplates.

Characterization of the materials

The crystal structure of the as-synthesized samples was identified using a PIXcel^{3D} X-ray diffractometer with Cu $K\alpha$ source. A field emission scanning

electron microscope (FE-SEM, S-4800, 15 kV) was used to observe the morphologies of the samples. The microstructure of the samples was investigated by using a Tecnai G2 F20 H-800 transmission electron microscope with an accelerating voltage of 200 kV. The carbon content of the samples was determined by thermogravimetric (TG) analysis. X-ray photoelectron spectroscopy of the samples was collected using an ESCALAB-250Xi spectrometer. The Raman spectra were obtained using a HORIBA LabRAM HR800 equipped with a 514-nm Ar-ion laser.

Electrochemical measurements

The electrochemical properties of the samples were performed using CR2032 coin cells. The electrode was prepared by mixing active materials, acetylene black and polyvinylidene fluoride (PVDF) in a weight ratio of 80:10:10 in N-methyl-2-pyrrolidone (NMP). The slurry of mixture was coated onto aluminum foils using a film-coating machine and dried at 110 °C for 12 h in vacuum condition. The dried film was pressed in a fixed pressure, and then, the electrode sheet was punched into disks with a diameter of 14 mm. The electrolyte was 1 M LiPF₆ in a mixture solution of ethylene carbonate (EC), dimethyl carbonate (DMC) and ethyl methyl carbonate (EMC) in a volume ratio of 1:1:1. The prepared electrode was used as the working electrode. The pure lithium plate served as the anode, and a polypropylene membrane (Celgard 2400) was used as the separator. The coin cells were assembled in an argon-filled glove box. Galvanostatic charge/discharge measurements were made on an Arbin battery testing system. Electrochemical impedance spectroscopy (EIS) testing was conducted using a Solartron electrochemical workstation with an AC signal of 5 mV and a frequency range from 10 mHz to 100 kHz. The cyclic voltammetry (CV) tests were also carried out using the Solartron electrochemical workstation at various scanning rates in the potential range of 3.0–4.3 V.

Results and discussion

Material characterization

XRD patterns of H-LNVP and R-LNVP samples are shown in Fig. 1a, b. All the diffraction peaks of the H-LNVP sample (Fig. 1a) could be indexed to a two-

phase mixture of R-LVP and M-LVP. According to Rietveld refinement, the mole ratio of M-LVP to R-LVP is 58:42. The lattice parameters of the M-LVP are $a = 8.664 \text{ \AA}$, $b = 12.212 \text{ \AA}$, $c = 0.8603 \text{ \AA}$, and those of the R-LVP are $a = b = 8.339 \text{ \AA}$, $c = 22.454 \text{ \AA}$, which are in good agreement with those of the previous studies [16, 18]. The obtained parameters are $R_{\text{exp}} = 3.03\%$, $R_{\text{wp}} = 6.03\%$ and $R_p = 4.62\%$, which represent the satisfactory quality of the Rietveld refinement. The R-LNVP sample (Fig. 1b) is nearly pure R-LVP phase with a space group of $R\bar{3}C$ analyzed by Rietveld refinement with satisfactory reliability factors ($R_{\text{exp}} = 2.07\%$, $R_{\text{wp}} = 4.98\%$ and $R_p = 3.5\%$). The unit cell parameters are $a = b = 8.341 \text{ \AA}$ and $c = 22.458 \text{ \AA}$, and the atomic positions of the R-LNVP sample are listed in Table 1. The absence of rhombohedral Na₃V₂(PO₄)₃ in these two samples suggests that small amount Na can replace completely Li of pristine LVP structure. No diffraction peaks of carbon phase are observed in the XRD patterns of these two samples, indicating that the residual carbon is amorphous. XPS measurements were made to study the content and oxidation states of the elements of the prepared samples, as displayed in Fig. 1(c). The peaks at the binding energy of 55.1, 133.6, 190.8, 285.4, 531.2 and 1071.2 eV corresponds to Li1s, P2p, P2s, C1s, O1s and Na1s, respectively. The high-resolution V2p_{3/2} XPS spectrum in Fig. 1d shows a peak at 516.9 eV, which represents the oxidation state of V³⁺ and is in good agreement with the previously reported papers [22, 23]. The content of Na in H-LNVP and R-LNVP determined by XPS is approximately identical, with a molar ratio value about 0.55 and 0.56, respectively. In order to identify the structural characteristics of the carbon coated on the surface of LNVP particles, Raman spectroscopy measurements were made, as shown in Fig. 1e. Two intense broad peaks located at about 1347 and 1586 cm⁻¹ in the Raman spectrum of the R-LNVP sample can be assigned to the disorder-induced phonon mode (D-band) and graphite band (G-band), respectively. The ratio of I_D/I_G is 0.97, indicating that a high graphitization degree of carbon existed in the carbon matrices [24]. The carbon content is determined to be around 6.5 and 8.9 wt% for the H-LNVP and R-LNVP samples (Fig. 4f), respectively, using the TG analysis technique.

Figure 2 shows SEM and TEM images of the samples. As illustrated in Fig. 2a, the H-LNVP sample consists of nano/micro-sized spheres. From Fig. 2b,

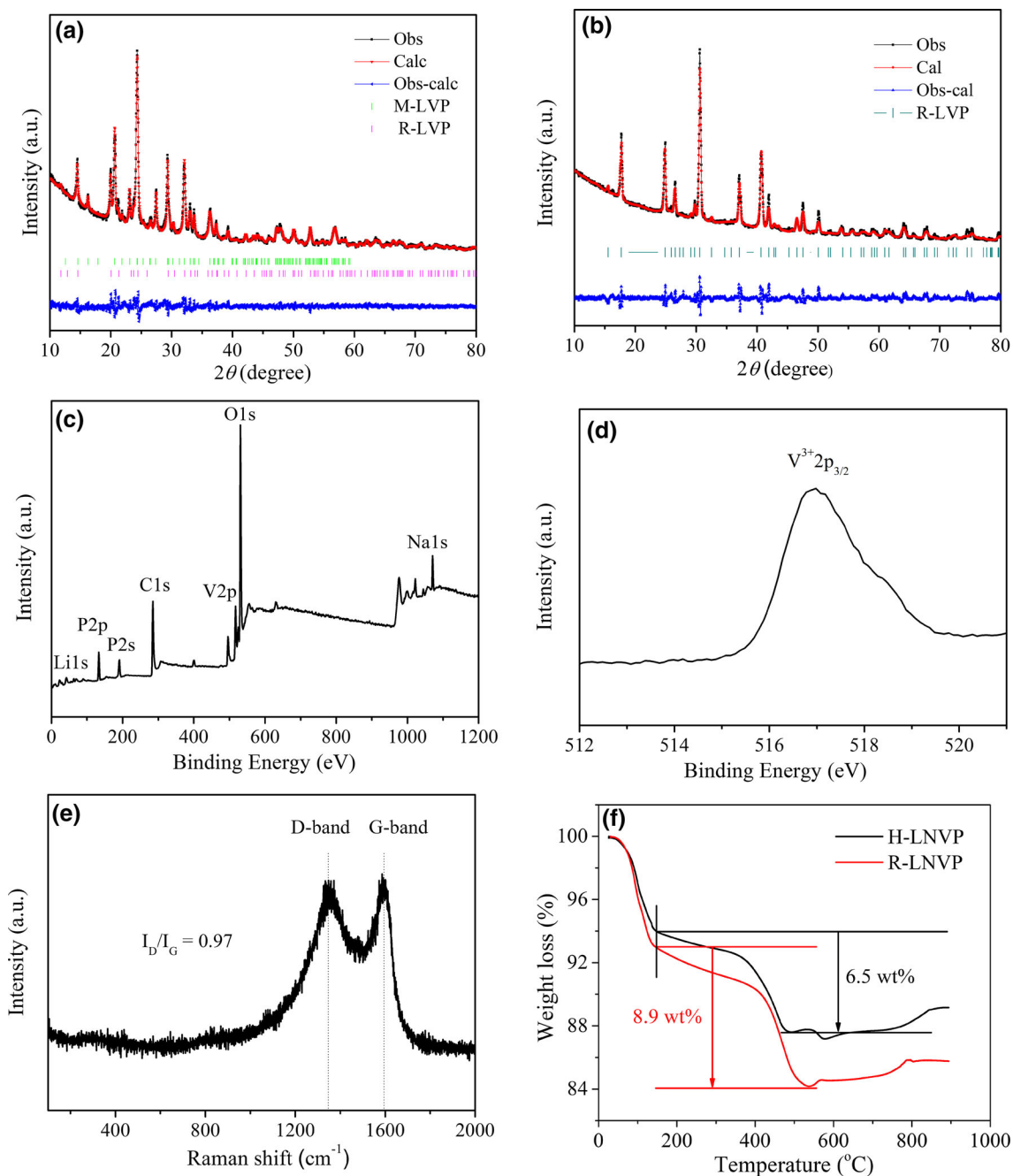


Figure 1 a, b XRD patterns of the H-LNVP and R-LNVP samples. c, d The whole XPS spectra and the $V2p_{3/2}$ XPS spectrum of the R-LNVP sample. e Raman spectra of the R-LNVP sample. f TG curves for the H-LNVP and R-LNVP samples.

the R-LNVP sample exhibits nanoplate-like particles with a thickness of about 20 nm and a width of around 500 nm. The morphology of two samples is confirmed by TEM (Fig. 2c, d) to be nano/microspheres and nanoplates, respectively. High-resolution TEM (HRTEM) images (Fig. 2e, f) reveal an amorphous carbon layer with a thickness of about 4.8 nm and 5.8 nm covering on the surface of the

H-LNVP and R-LNVP particles, which is expected to provide a high electronic conductivity to the materials. The characteristic of two-phase coexistence in the H-LNVP sample is verified in Fig. 2e. The lattice fringes with a spacing of 0.440 and 0.373 nm correspond to the (012) planes of M-LVP and the (113) planes of R-LVP, respectively. In addition, the two-phase boundary is clearly observed in the HRTEM

Table 1 Atomic positions of the R-LNVP sample deduced from Rietveld refinement of the XRD data

Atom	Wyckoff site	<i>x</i>	<i>y</i>	<i>z</i>
Li1	18	0.34102	0.02389	0.38194
V1	18	0	0	0.14606
V2	18	0	0	0.65285
P1	18	0.29231	0.00187	0.25128
O1	18	0.19150	− 0.00961	0.19192
O2	18	0.76558	0.91257	0.69887
O3	18	0.24342	0.80066	0.26590
O4	18	0.50056	0.87963	0.26594

image of the H-LNVP sample. In contrast, a typical well-crystalline R-LVP is clearly identified in the R-LNVP sample. As shown in Fig. 2f, a lattice fringe spacing of 0.433 nm in the single-phase region is well matched to that of the (110) planes of R-LVP.

Electrochemical properties of the samples

CV curves of two samples were obtained at a scanning rate of 0.1 mV s^{−1} in the potential range of 3.0–4.3 V, as shown in Fig. 3a. Three anodic peaks at around 3.61, 3.69 and 4.1 V for the H-LNVP sample correspond to the extraction of lithium ion in the monoclinic phase, while the anodic peak at 3.82 V is attributed to the extraction reaction of lithium ions in the rhombohedral phase [14, 25]. Four corresponding cathodic peaks appear around 3.55, 3.63, 3.639 and 4.03 V, respectively. CV curve demonstrates the coexistence of monoclinic and rhombohedral phases in the H-LNVP sample. In contrast to the H-LNVP sample, the R-LNVP sample shows a pair of sharp redox peaks at around 3.81/3.69 V relating to the insertion/extraction of lithium ions in the rhombohedral phase and three very small auxiliary redox peaks caused by the insertion/extraction of lithium ions in the monoclinic phase, indicating that the R-LNVP sample consists of rhombohedral LVP and a negligible amount of monoclinic LVP. According to the CV curve, the mole ratio of R-LVP to M-LVP is estimated to be 95:5.

Figure 3b, c displays the CV curves of the H-LNVP and R-LNVP samples at various scanning rates of 0.1, 0.2, 0.5, 1 and 2 mV s^{−1}, respectively. Even at a relatively high scanning rate (2 mV s^{−1}), the well-defined and symmetrical redox peaks can be observed, implying the good lithium intercalation reversibility

and rate performance of the samples. As shown in Fig. 3d, the highest oxidation peak current has a linear relationship with the square root of scanning rate, which is indicative of electrode reaction controlled by diffusion [26]. The lithium-ion diffusion coefficient *D* (cm² s^{−1}) can be calculated by the following Randles-Sevcik Eq. (1) [27]:

$$i_p = (2.69 \times 10^5) n^{3/2} A D^{1/2} C_{Li}^* v^{1/2} \quad (1)$$

where *i_p* is the peak current (A), *n* is the number of electrons involved during the redox process, *A* is the surface area of electrode (cm²), *C_{Li}^{*}* is the concentration of lithium ions in the electrode (mol cm^{−3}), *v* is the scan rate (V s^{−1}), and *D* is the diffusion coefficient of lithium ions (cm² s^{−1}). Based on Eq. (1) and the slope of *i_p* versus *v*^{1/2} plots in Fig. 3d, the chemical diffusion coefficient of lithium ion in the H-LNVP and R-LNVP samples is calculated to be 5.06 × 10^{−10} and 1.01 × 10^{−9} cm² s^{−1}, respectively. The R-LNVP sample has a higher Li-ion chemical diffusion coefficient than the H-LNVP sample and LVP nanocrystals (10^{−10} cm² s^{−1}) [10], indicating better rate capability. It is resulted from a larger free volume of the interstitial space in rhombohedral LVP, supplying a faster lithium-ion movement [16].

The electrochemical performance of two samples was firstly evaluated by galvanostatic charge/discharge tests at 1 C (1 C = 133 mA g^{−1}) in the potential range of 3.0–4.3 V. Figure 4a, b presents the charge/discharge curves of the H-LNVP and R-LNVP samples. The H-LNVP sample exhibits four pairs of charge/discharge plateaus, which agrees well with the redox peaks in the CV curves. The plateaus around 3.6, 3.68 and 4.10 V correspond to the reversible reaction of the lithium ions in M-LVP, and the plateau near 3.76 V is assigned to lithium-ion insertion/extraction in R-LVP. In comparison, the R-LNVP sample shows clearly a pair of flat charge/discharge platforms at 3.77/3.72 V, which is attributed to the V³⁺/V⁴⁺ redox couple in R-LVP [14, 16, 19]. The corresponding cycle performance of the two samples is presented in Fig. 4c. Both samples deliver high capacities and excellent cycling stability. An initial discharge capacity of the H-LNVP and R-LNVP samples is 115.9 and 121.6 mAh g^{−1}, and a capacity retention is 100 and 95.6% after 200 cycles, respectively. Except the first several cycles, the coulombic efficiencies of two samples are close to 100% in the whole cycling processes. In order to evaluate objectively the superiority of the R-LNVP

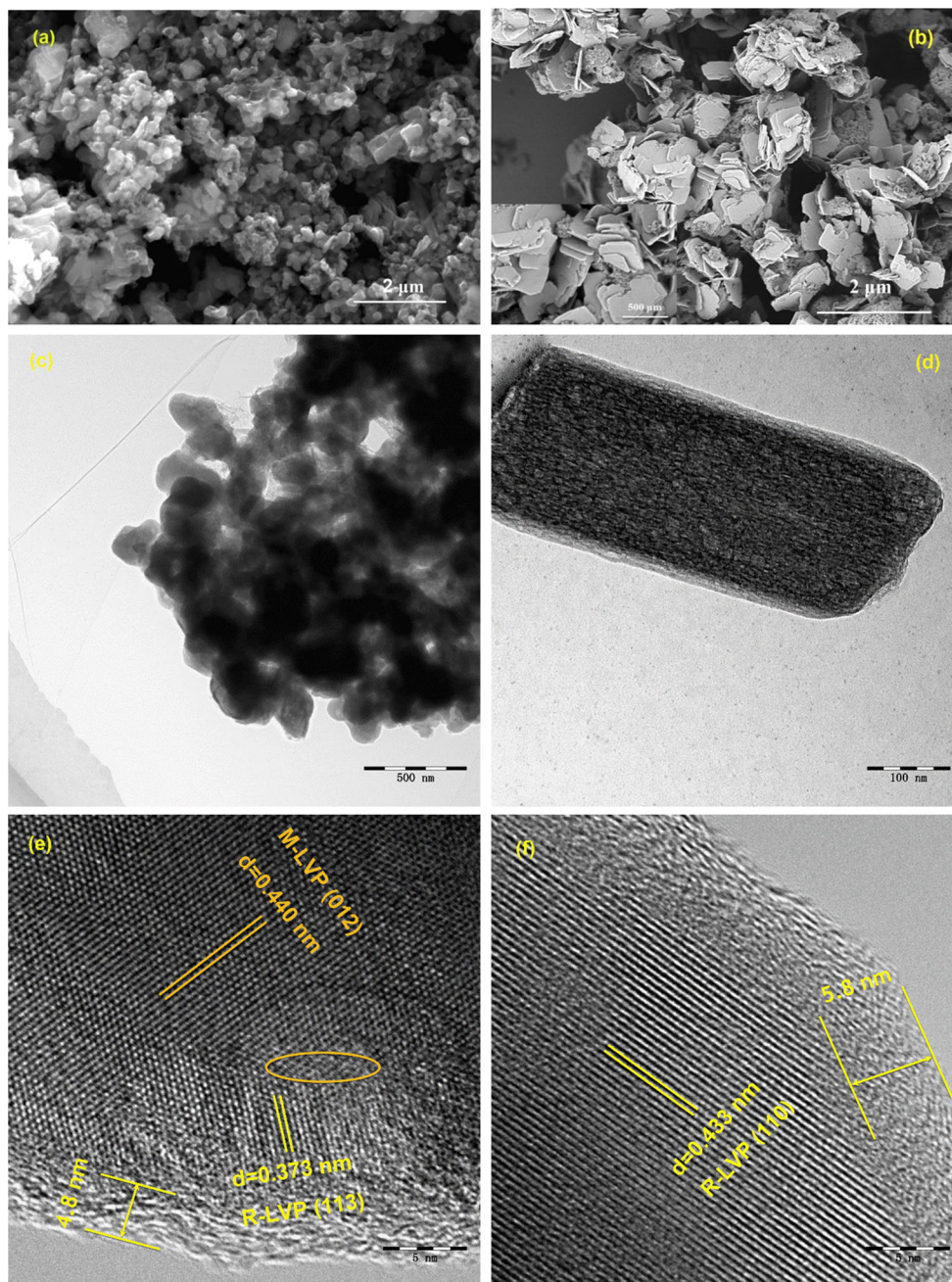


Figure 2 SEM, TEM and HRTEM images of **a, c, e** the H-LNVP and **b, d, f** R-LNVP samples.

sample, a comparison of cycle performance of the H-LNVP and R-LNVP samples with same carbon content (8.9 wt%) is carried out, as illustrated in Fig. 4c. The H-LNVP sample (8.9 wt%C) was prepared by adding 2.4 wt% conductive carbon (acetylene black) to the H-LNVP sample (6.5 wt%C) and mixing uniformly. The capacities and cycle performance were investigated by charge–discharge testing at 1 C. The H-LNVP sample (8.9 wt%C) shows an

initial discharge capacity of 117.5 mAh g^{-1} , which is inferior to that of the R-LNVP sample (121.6 mAh g^{-1}). In addition, the capacity retention of the H-LNVP sample (8.9 wt%C) is a little lower than that of the H-LNVP sample (6.5 wt%C). The results indicate that the effect of the increasing small carbon content (2.4 wt%) on the electrochemical performance of the samples is ignorable.

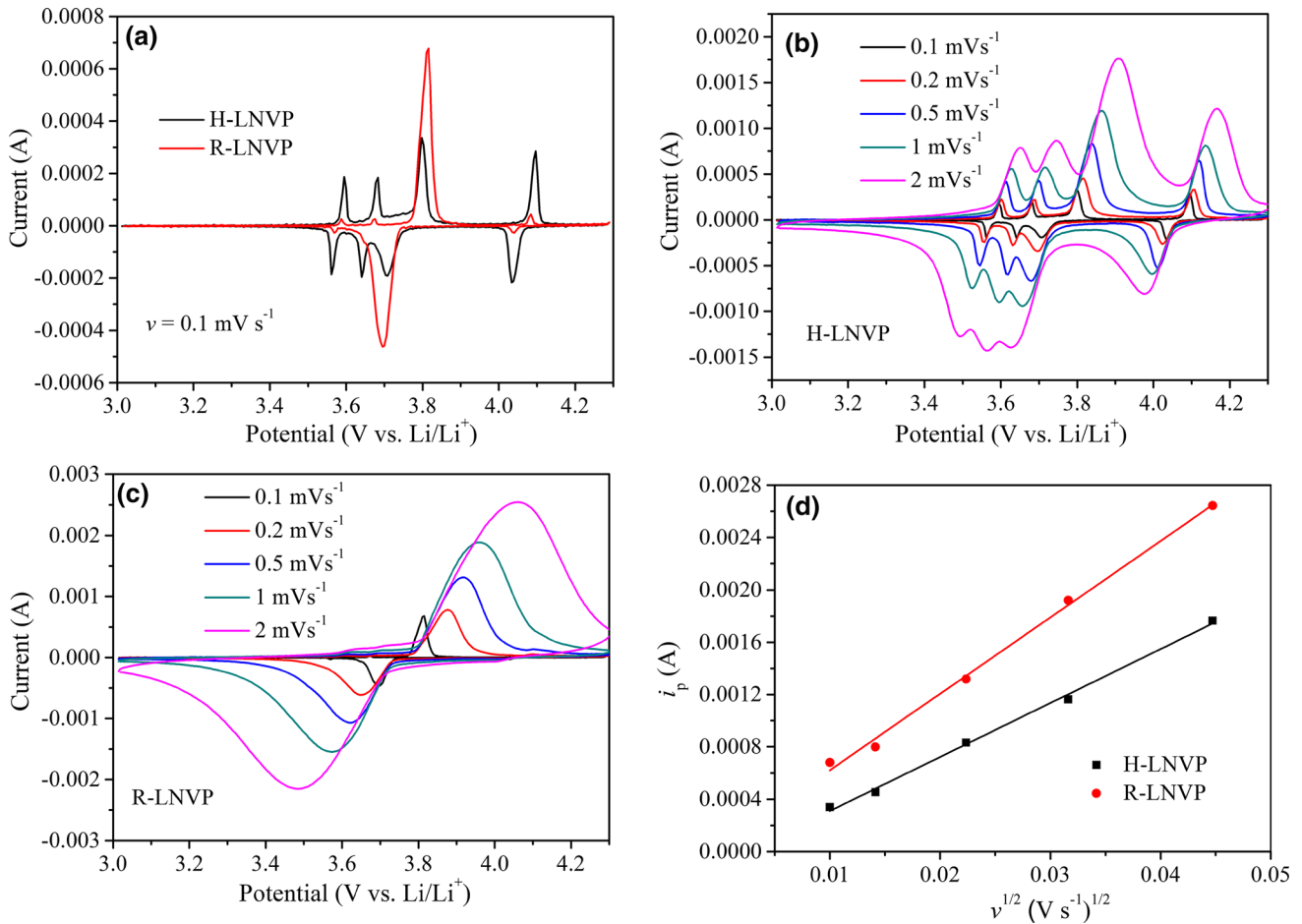


Figure 3 a Cyclic voltammograms of the H-LNVP and R-LNVP samples at a scanning rate of 0.1 mV s^{-1} in the potential range of 3.0–4.3 V. b, c Cyclic voltammograms of two samples at various

scanning rates. d A linear relationship between the oxidation peak current and the square root of scanning rate for two samples.

To evaluate the rate capability, the H-LNVP and R-LNVP samples are also tested at various current rates of 0.1 C, 0.5 C, 1 C, 5 C, 10 C and 20 C in the potential range of 3.0–4.3 V. The rate capability of two samples is displayed in Fig. 4d. The discharge capacities of the H-LNVP sample are 114.1, 115.6, 113.8, 105.4, 97.4 and 80.1 mAh g^{-1} at 0.1 C, 0.5 C, 1 C, 5 C, 10 C and 20 C, respectively. Compared with the H-LNVP sample, the R-LNVP sample exhibits higher discharge capacities of 121.6, 119.3, 115.6, 108.4, 102.9 and 94.7 mAh g^{-1} under the same testing procedures, indicating an outstanding rate capability. After 55 cycles, the current density recovers to 0.5 C; the discharge capacity of the R-LNVP sample can remain 116.7 mAh g^{-1} , as high as 96.0% of the first capacity (121.6 mAh g^{-1}). The gravimetric energy density of the R-LNVP sample (451.5 Wh kg^{-1}) is higher than that of the H-LNVP sample (435.1 Wh

kg^{-1}) and LiMn_2O_4 ($\sim 430 \text{ Wh kg}^{-1}$) [28]. The remarkable rate capability of the R-LNVP sample may be attributed to the synergetic effect of nanoplate-like structure and stable rhombohedral LVP. Compared with spherical H-LNVP, the R-LNVP nanoplates can provide a higher surface area and a shorter lithium-ion diffusion path, in favor of improving the rate capability. The stabilized NASICON framework of rhombohedral LVP could provide a better lithium-ion transport in LVP, leading to enhance the rate capability and cycle stability [16]. Furthermore, the uniform and thick carbon coating layer on the surface of the R-LNVP particles effectively increases its electronic conductivity and improves the electrochemical performance.

The high-rate long-term cycle stability of the H-LNVP and R-LNVP samples at 10 C is shown in Fig. 4e. The R-LNVP sample exhibits higher cycle

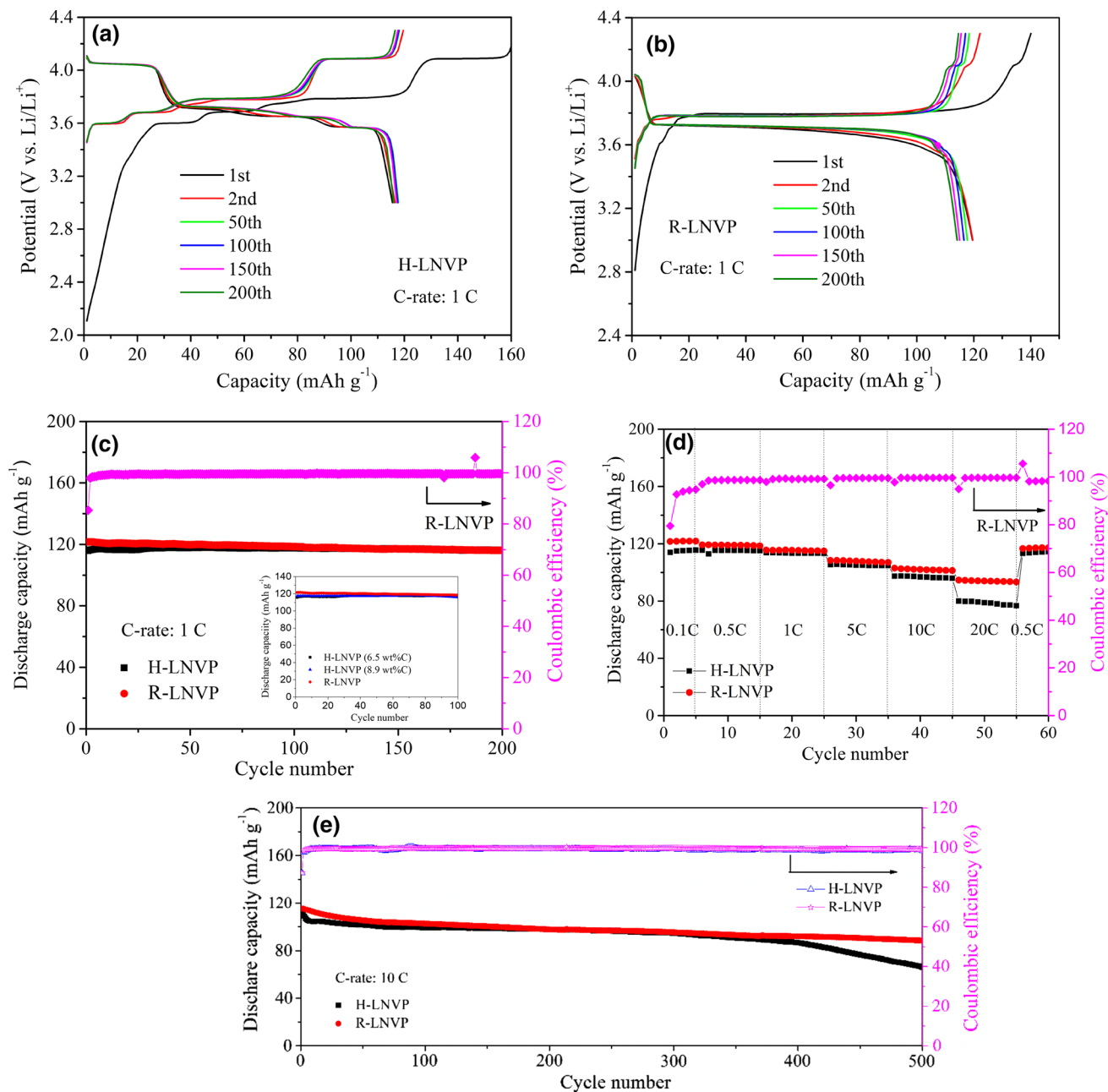


Figure 4 The electrochemical performance of the H-LNVP and R-LNVP samples. **a, b** The charge–discharge profiles of at a rate of 1 C in the voltage of 3.0–4.3 V. **c** Cycle performances at 1 C rate. **d** Rate capability. **e** The long-term cycle stability at 10 C.

stability than the H-LNVP sample, with an initial discharge capacity of 115.3 mAh g^{-1} and a capacity retention of 76.7% after 500 cycles. The excellent long-term cycle performance of the R-LNVP sample is due to the synergistic effect of nanoplate-like structure, stable rhombohedral LVP and uniform carbon coating layer. The electrochemical performance of the R-LNVP sample is comparable to previous reported plate-like V-based phosphate cathodes (Table 2),

confirming the superiority of the R-LNVP sample developed in this work.

To further understand lithium-ion insertion/extraction kinetics of the samples, EIS spectra of two samples were tested in fully discharge state of the cells after different cycles at 1 C. The AC voltage amplitude of 5 mV was employed in a frequency range of 10 mHz–100 kHz. From Fig. 5, all EIS spectra consist of a depressed semicircle at the high-

Table 2 A comparison of the electrochemical performance of R-LNVP@C nanoplates in this work and previous reported plate-like V-based phosphate cathodes

Cathode materials	Discharge capacity at low rate (mAh g ⁻¹)	Discharge capacity at high rate (mAh g ⁻¹)	Long-term cycle life at high rate	References
Li ₃ V ₂ (PO ₄) ₃ /C submicron sheets	130.0 (0.2 C)	106.0 (10 C)	83.0% (800 cycles)	[9]
Carbon-coated rhombohedral Li ₂ NaV ₂ (PO ₄) ₃ nanoflake	92 (0.4 C)	55 (12 C)	–	[21]
Plate-like Li ₃ V ₂ (PO ₄) ₃ /C	131.6 (0.1 C)	125.2 (3 C)	89.3% (500 cycles)	[25]
Li ₃ V ₂ (PO ₄) ₃ /graphene nanosheets	130 (0.1 C)	17 (50 C)	46 mAh g ⁻¹ (1000 cycles)	[26]
Carbon-coated Li ₃ V ₂ (PO ₄) ₃ nanoplates	129.9 (0.1 C)	125.1 (1 C)	91.4% (200 cycles)	[29]
Li ₃ V ₂ (PO ₄) ₃ /C nanoflakes	129.6 (0.1 C)	120 (1 C) 96 (50 C)	–	[30]
Li ₃ V ₂ (PO ₄) ₃ /rGO&C sheets	ca. 134 (0.5 C)	131 (1 C) 118 (5 C)	95.4% (100 cycles) 89.2% (1000 cycles)	[31]
R-Li _{2.4} Na _{0.6} V ₂ (PO ₄) ₃ @C nanoplates	121.6 (0.1 C)	121.6 (1 C) 116.9 (10 C)	95.6% (200 cycles) 76.7% (500 cycles)	This work

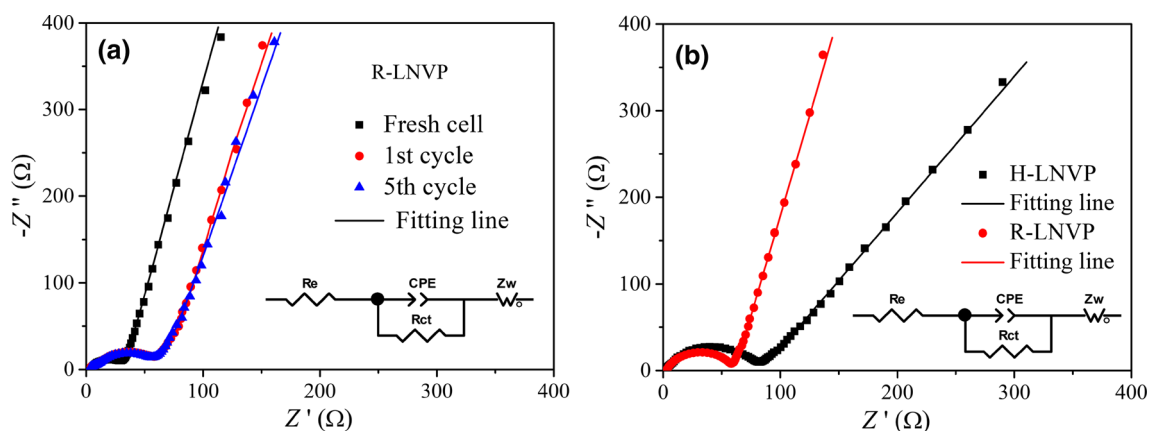


Figure 5 Impedance spectra of two samples. **a** Nyquist plots of the R-LNVP sample under different cycles at 1 C. **b** Nyquist plots of two samples after the 200th cycle at 1 C.

frequency region and a sloping line at the low-frequency region. All the EIS spectra were simulated by an equivalent circuit model using the Zview program [32]. The semicircle at the high-frequency region is related to the charge transfer resistance (R_{ct}). The sloping line in the low-frequency region represents the diffusion impedance of lithium ions in active

materials. The fitting results are listed in Table 3. The R_{ct} value of the R-LNVP fresh cell is 24 Ω and then increases to 54, 52 and 50 Ω after 1, 5 and 200 cycles, respectively. The large increase in R_{ct} value in the first cycle can be attributed to the formation of solid electrolyte interface (SEI) film [11], then slightly decreases after 5 cycles owing to the perfect carbon

Table 3 The fitting results of EIS spectra for the H-LNVP and R-LNVP samples

Sample	H-LNVP	R-LNVP			
		Fresh cell	First cycle	Fifth cycle	200th cycle
R_s (Ω)	1.2	3.3	3.9	3.0	2.5
R_{ct} (Ω)	70	24	54	52	50

coating layer and keeps almost unchanged over 200 cycles due to the stable rhombohedral structure. It can be found that the R_{ct} value of the R-LNVP sample (50 Ω) is lower than that of the H-LNVP sample (70 Ω), suggesting the nanoplate-structured R-LNVP has fast charged species transport and enhanced rate capability.

Conclusions

In summary, rhombohedral $\text{Li}_{2.4}\text{Na}_{0.6}\text{V}_2(\text{PO}_4)_3@\text{C}$ nanoplates have been successfully synthesized by a simple sol-gel method. For comparison, hybrid-phase $\text{Li}_{2.4}\text{Na}_{0.6}\text{V}_2(\text{PO}_4)_3@\text{C}$ nano/microspheres have also been prepared by a solvothermal method. As cathode materials for lithium-ion batteries, the rhombohedral $\text{Li}_{2.4}\text{Na}_{0.6}\text{V}_2(\text{PO}_4)_3@\text{C}$ nanoplates show superior electrochemical properties than the hybrid-phase $\text{Li}_{2.4}\text{Na}_{0.6}\text{V}_2(\text{PO}_4)_3@\text{C}$ nano/microspheres. Rhombohedral $\text{Li}_{2.4}\text{Na}_{0.6}\text{V}_2(\text{PO}_4)_3@\text{C}$ nanoplates deliver a high initial discharge capacity of 121.6 mAh g^{-1} and an excellent capacity retention of 95.6% after 200 cycles at 1 C in the potential range of 3.0–4.3 V. Even at a high rate of 10 C, they also exhibit an initial discharge capacity of 115.3 mAh g^{-1} and a capacity retention of 76.7% after 500 cycles. The outstanding electrochemical performance is ascribed to the synergetic effect of nanoplate structure, stable rhombohedral LVP phase and uniform carbon coating layer.

Acknowledgements

This work was financially supported by the National Natural Science Foundation of China (Nos. 51661009, 21363005 and 51371061) and the Natural Science Foundation of Guangxi Province (2016GXNSFGA380001).

References

- [1] Goodenough JB, Kim Y (2010) Challenges for rechargeable Li batteries. *Chem Mater* 22(3):587–603
- [2] Goodenough JB, Park K-S (2013) The Li-ion rechargeable battery: a perspective. *J Am Chem Soc* 135(4):1167–1176
- [3] Nitta N, Wu F, Lee JT, Yushin G (2015) Li-ion battery materials: present and future. *Mater Today* 18(5):252–264
- [4] Yuan L-X, Wang Z-H, Zhang W-X, Hu X-L, Chen J-T, Huang Y-H, Goodenough JB (2011) Development and challenges of LiFePO_4 cathode material for lithium-ion batteries. *Energy Environ Sci* 4(2):269–284
- [5] Malik R, Abdellahi A, Ceder G (2013) A critical review of the Li insertion mechanisms in LiFePO_4 electrodes. *J Electrochem Soc* 160(5):A3179–A3197
- [6] Pivko M, Bele M, Tchernychova E, Logar NZ, Dominko R, Gaberscek M (2012) Synthesis of nanometric LiMnPO_4 via a two-step technique. *Chem Mater* 24(6):1041–1047
- [7] Aravindan V, Gnanaraj J, Lee Y-S, Madhavi S (2013) LiMnPO_4 —A next generation cathode material for lithium-ion batteries. *J Mater Chem A* 1(11):3518–3539
- [8] Oh S-M, Myung S-T, Sun Y-K (2012) Olivine LiCoPO_4 -carbon composite showing high rechargeable capacity. *J Mater Chem* 22(30):14932–14937
- [9] Cheng Y, Ni X, Feng K, Zhang H, Li X, Zhang H (2016) Phase-change enabled 2D $\text{Li}_3\text{V}_2(\text{PO}_4)_3/\text{C}$ submicron sheets for advanced lithium-ion batteries. *J Power Sources* 326:203–210
- [10] Wang L, Bai J, Gao P, Wang X, Looney JP, Wang F (2015) Structure tracking aided design and synthesis of $\text{Li}_3\text{V}_2(\text{PO}_4)_3$ nanocrystals as high-power cathodes for lithium ion batteries. *Chem Mater* 27(16):5712–5718
- [11] Zhang L-L, Li Z, Yang X-L, Ding X-K, Zhou Y-X, Sun H-B, Tao H-C, Xiong L-Y, Huang Y-H (2017) Binder-free $\text{Li}_3\text{V}_2(\text{PO}_4)_3/\text{C}$ membrane electrode supported on 3D nitrogen-doped carbon fibers for high-performance lithium-ion batteries. *Nano Energy* 34:111–119
- [12] Rajagopalan R, Zhang L, Dou SX, Liu H (2016) Lyophilized 3D lithium vanadium phosphate/reduced graphene oxide electrodes for super stable lithium ion batteries. *Adv Energy Mater* 6(1):1501760-1–1501760-8
- [13] Huang H, Yin SC, Kerr T, Taylor N, Nazar LF (2002) Nanostructured composites: a high capacity, fast rate $\text{Li}_3\text{V}_2(\text{PO}_4)_3/\text{carbon}$ cathode for rechargeable lithium batteries. *Adv Mater* 14(21):1525–1528
- [14] Jian Z, Han W, Liang Y, Lan Y, Fang Z, Hu Y-S, Yao Y (2014) Carbon-coated rhombohedral $\text{Li}_3\text{V}_2(\text{PO}_4)_3$ as both cathode and anode materials for lithium-ion batteries: electrochemical performance and lithium storage mechanism. *J Mater Chem A* 2(47):20231–20236
- [15] Rui X, Yan Q, Skyllas-Kazacos M, Lim TM (2014) $\text{Li}_3\text{V}_2(\text{PO}_4)_3$ cathode materials for lithium-ion batteries: a review. *J Power Sources* 258:19–38
- [16] Lu Y, Wang L, Song J, Zhang D, Xu M, Goodenough JB (2013) Aluminum-stabilized NASICON-structured $\text{Li}_3\text{V}_2(\text{PO}_4)_3$. *J Mater Chem A* 1(1):68–72
- [17] Yin SC, Grondy H, Strobel P, Anne M, Nazar LF (2003) Electrochemical property: structure relationships in

- monoclinic $\text{Li}_{3-y}\text{V}_2(\text{PO}_4)_3$. *J Am Chem Soc* 125(34): 10402–10411
- [18] Gaubicher J, Wurm C, Goward G, Masquelier C, Nazar L (2000) Rhombohedral form of $\text{Li}_3\text{V}_2(\text{PO}_4)_3$ as a cathode in Li-ion batteries. *Chem Mater* 12(11):3240–3242
- [19] Zhang Y, Nie P, Shen L, Xu G, Deng H, Luo H, Zhang X (2014) Rhombohedral NASICON-structured $\text{Li}_2\text{NaV}_2(\text{PO}_4)_3$ with single voltage plateau for superior lithium storage. *RSC Adv* 4(17):8627–8631
- [20] Wang W, Chen Z, Zhang J, Dai C, Li J, Ji D (2013) A comparative structural and electrochemical study of monoclinic $\text{Li}_3\text{V}_2(\text{PO}_4)_3/\text{C}$ and rhombohedral $\text{Li}_{2.5}\text{Na}_{0.5}\text{V}_{(2-2x/3)}\text{Ni}_x(\text{PO}_4)_3/\text{C}$. *Electrochim Acta* 103:259–265
- [21] Alfaruqi MH, Islam S, Song J, Kim S, Pham DT, Jo J, Kim S, Baboo JP, Putro DY, Mathew V, Kim J (2017) Carbon-coated rhombohedral $\text{Li}_2\text{NaV}_2(\text{PO}_4)_3$ nanoflake cathode for Li-ion battery with excellent cycleability and rate capability. *Chem Phys Lett* 681:44–49
- [22] Cui K, Hu S, Li Y (2016) Nitrogen-doped graphene nanosheets decorated $\text{Li}_3\text{V}_2(\text{PO}_4)_3/\text{C}$ nanocrystals as high-rate and ultralong cycle-life cathode for lithium-ion batteries. *Electrochim Acta* 210:45–52
- [23] Sun P, Zhao X, Chen R, Chen T, Ma L, Fan Q, Lu H, Hu Y, Tie Z, Jin Z, Xu Q, Liu J (2016) $\text{Li}_3\text{V}_2(\text{PO}_4)_3$ encapsulated flexible free-standing nanofabric cathodes for fast charging and long life-cycle lithium-ion batteries. *Nanoscale* 8(14):7408–7415
- [24] Chen L, Yan B, Xu J, Wang C, Chao Y, Jiang X, Yang G (2015) Bicontinuous structure of $\text{Li}_3\text{V}_2(\text{PO}_4)_3$ clustered via carbon nanofiber as high-performance cathode material of Li-Ion batteries. *ACS Appl Mater Interfaces* 7(25):13934–13943
- [25] Qiao YQ, Wang XL, Mai YJ, Xiang JY, Zhang D, Gu CD, Tu JP (2011) Synthesis of plate-like $\text{Li}_3\text{V}_2(\text{PO}_4)_3/\text{C}$ as a cathode material for Li-ion batteries. *J Power Sources* 196(20):8706–8709
- [26] Liu H, Yang G, Zhang X, Gao P, Wang L, Fang J, Pinto J, Jiang X (2012) Kinetics of conventional carbon coated- $\text{Li}_3\text{V}_2(\text{PO}_4)_3$ and nanocomposite $\text{Li}_3\text{V}_2(\text{PO}_4)_3/\text{graphene}$ as cathode materials for lithium ion batteries. *J Mater Chem A* 22(22):11039–11047
- [27] Zuo Z-L, Deng J-Q, Pan J, Luo W-B, Yao Q-R, Wang Z-M, Zhou H-Y, Liu H-K (2017) High energy density of $\text{Li}_{3-x}\text{Na}_x\text{V}_2(\text{PO}_4)_3/\text{C}$ cathode material with high rate cycling performance for lithium-ion batteries. *J Power Sources* 357:117–125
- [28] Fang C, Huang Y, Zhang W, Han J, Deng Z, Cao Y, Yang H (2016) Routes to high energy cathodes of sodium-ion batteries. *Adv Energy Mater* 6(5):1501727-1–1501727-8
- [29] Teng F, Hu Z-H, Ma X-H, Zhang L-C, Ding C-X, Yu Y, Chen C-H (2013) Hydrothermal synthesis of plate-like carbon-coated $\text{Li}_3\text{V}_2(\text{PO}_4)_3$ and its low temperature performance for high power lithium ion batteries. *Electrochim Acta* 91:43–49
- [30] Wang Y, Tang Y, Zhong B, Liu H, Zhong Y, Guo X (2014) Facile synthesis of $\text{Li}_3\text{V}_2(\text{PO}_4)_3/\text{C}$ nano-flakes with high-rate performance as cathode material for Li-ion battery. *J Solid State Electrochem* 18(1):215–221
- [31] Wei Q, Xu Y, Li Q, Tan S, Ren W, An Q, Mai L (2016) Novel layered $\text{Li}_3\text{V}_2(\text{PO}_4)_3/\text{rGO}\&\text{C}$ sheets as high-rate and long-life lithium ion battery cathodes. *Chem Commun* 52(56):8730–8732
- [32] Wang S, Zhang Z, Jiang Z, Deb A, Yang L, S-i Hirano (2014) Mesoporous $\text{Li}_3\text{V}_2(\text{PO}_4)_3@\text{CMK-3}$ nanocomposite cathode material for lithium ion batteries. *J Power Sources* 253:294–299